C. R. Mecanique 344 (2016) 335–354

Contents lists available at ScienceDirect

Comptes Rendus Mecanique

www.sciencedirect.com

Computational simulation of manufacturing processes

Some insights on the modelling of chip formation and its morphology during metal cutting operations

Tarek Mabrouki [a,*], Cédric Courbon [b], Yancheng Zhang [c], Joël Rech [b], Daniel Nélias [c], Muhammad Asad [d], Hédi Hamdi [b], Salim Belhadi [e], Ferdinando Salvatore [b]

[a] Université de Tunis El Manar, École nationale d'ingénieurs de Tunis (ENIT), 1002 Tunis, Tunisia
[b] Université de Lyon, CNRS, École nationale d'ingénieurs de Saint-Étienne, LTDS UMR5513, 42023 Saint-Étienne cedex 2, France
[c] Université de Lyon, CNRS, INSA-Lyon, LaMCoS UMR5259, 69621 Villeurbanne cedex, France
[d] Department of Industrial & Mechanical Engineering, School of Engineering, University of Management & Technology, 54770 Lahore, Pakistan
[e] Mechanics and Structures Research Laboratory (LMS), 8 May 1945 University of Guelma, P.O. Box 401, 24000, Algeria

ARTICLE INFO

Article history:
Received 10 May 2015
Accepted 22 August 2015
Available online 2 March 2016

Keywords:
Cutting simulation
Plasticity
Damage
Chip formation
Size effect

ABSTRACT

The present paper deals with the mechanisms of chip formation during cutting operations. It deals with some experiments characterising the chip morphologies and microstructure chip investigations under high loadings. In this contribution, mechanisms of chip segmentation are presented. The effect of cutting conditions on cutting forces is treated. Consequently, the chip segmentation phenomenon was correlated to cutting forces evolutions. Also, an investigation on chip strain localisation is carried out. Numerical simulations dealing with chip formation and considering thermomechanical phenomena are also presented. Some numerical results related to chip formation based on the theory of strain gradient plasticity are also discussed. Moreover, the effect of machining system stiffness on chip segmentation is analysed.

1. Introduction

In the framework of machining, it is essential to have predictive approaches helping to complement the knowledge necessary for a comprehensive and industrial understanding of the process. There are various experimental methods dedicated to cutting studies in terms of tool wear investigation [1,2], evolution of cutting forces, etc. In particular the investigation of chip formation such as the quick-stop testing, temperature measurement systems or methods of chip visualisation were proposed, etc. However, these methods have limitations because of their costs and also because of difficulties in providing a comprehensive and relevant understanding.

It is important to note that analytical cutting models are still essentially driving from experimentation. Some parameters and coefficients of these experimental models are obtained with tests codified both by the scientific community and the industrial sector concerned. Measurement methods are standardised to allow their transmission and their interchangeability. Analytical cutting models of a two-dimensional representation (orthogonal case) are elaborated for these experimental scientific approaches. These empirical analytical models are usually defined for a given Couple Workpiece/Tool

* Corresponding author.
E-mail address: tarek.mabrouki@enit.rnu.tn (T. Mabrouki).

http://dx.doi.org/10.1016/j.crme.2016.02.003
1631-0721/

Nomenclature

List of symbols

A	Initial yield stress (MPa)
a_p	Cutting depth or axial depth of cut (mm)
B	Hardening modulus (MPa)
b	Burgers vector (nm)
C	Strain rate dependency coefficient
C_{eq}	Equivalent linear damping of machining system ($kg\,s^{-1}$)
C_p	Specific heat ($J\,kg^{-1}\,K^{-1}$)
D	Overall damage variable
$D_1 \dots D_5$	Coefficients of Johnson–Cook material shear failure initiation criterion
D_T	Tool diameter in milling (mm)
E	Young's modulus (MPa)
f	Feed rate (mm/rev)
F_i	Cutting force (N) along various axis (i = axial, radial, tangential)
G	Shear modulus (MPa)
G_f	Fracture energy (N/m)
K_C	Fracture toughness ($MPa\sqrt{m}$)
K_r	Insert attack angle or entering angle (deg)
k_{eq}	Equivalent linear stiffness of machining system (N/m)
l	Intrinsic characteristic length of the cut material
L_C	Tool rake face-chip contact length (μm)
m	Thermal softening coefficient
m_{eq}	Equivalent moving mass (kg)
N	Spindle rotation frequency (rev/min)
n	Work-hardening exponent
P	Hydrostatic pressure (MPa)
r_β	Tool hone edge radius (μm)
T	Temperature at a given calculation instant (°C)
T_m	Melting temperature (°C)
T_0	Room temperature (°C)
$\bar{u}$	Equivalent plastic displacement (mm)
$\bar{u}_f$	Equivalent plastic displacement at failure (mm)
Δu	Relative displacement of spring element (mm)
V_C	Cutting speed (m/min)
$P/\bar{\sigma}_{JC}$	Stress triaxiality
$\bar{\varepsilon}^p$	Equivalent plastic strain
$\bar{\varepsilon}_f$	Equivalent plastic strain at failure
$\Delta\bar{\varepsilon}^p$	Equivalent plastic strain increment
σ_n	Normal stress (MPa)
$\bar{\varepsilon}_{0i}$	Plastic strain at damage initiation
$\dot{\bar{\varepsilon}}^p$	Plastic strain rate (s^{-1})
$\dot{\bar{\varepsilon}}^p_0$	Reference strain rate ($10^{-3}\ s^{-1}$)
$\bar{\sigma}$	von Mises plastic equivalent stress (MPa)
σ_y	Yield stress (MPa)
τ_f	Friction shear stress (MPa)
$\bar{\sigma}_{JC}$	Johnson–Cook equivalent stress (MPa)
τ_Y	Yield shear stress (MPa)
λ	Edge inclination angle (deg)
α_t	Taylor's constant
α_o	Flank/clearance angle (deg)
γ_o	Rake/cutting angle (deg)
χ_r	Edge entering angle (deg)
μ	Friction coefficient
ω	Damage initiation criterion
r_ϵ	Insert radius (mm)
ζ_{eq}	Equivalent damping ratio of the machining system
η	Strain gradient coefficient
λ	Thermal conductivity ($W\,m^{-1}\,K^{-1}$)
ρ	Density of the material ($kg\,m^{-3}$)
χ	Geometric factor defining the density of GND
ν	Poisson's ratio

List of abbreviations

ALE	Arbitrary Lagrangian–Eulerian formulation
CWT	Couple Workpiece/Tool
FE	Finite Element
$F_{Seg\text{-}signal}$	Chip segmentation measured by gathering signal (Hz)
$F_{Seg\text{-}geo}$	Chip segmentation measured on chip morphology (Hz)
GND	Geometrically Necessary Dislocation
HDC	Hybrid Dynamic Cutting model
JC	Johnson–Cook
rpm	Revolution per minute
SG	Strain Gradient
UCT	Uncut Chip Thickness
w/o	Without
2D	Two dimensional model
PSZ	Chip Primary Shear Zone
SSZ	Chip Secondary Shear Zone

(*CWT*) methodology [3] and are exploited to obtain a range of optimal cutting parameters with a minimum of experiments. Nevertheless, it is underlined that cutting experimentation is always costly, due to the need for specialised equipment such as dynamometers, accelerometers, and data acquisition systems. Generally, a complete *CWT* is accomplished when it is necessary to determine ranges of cutting parameters for achieving a given quality criteria or a production cost function.

In this context, the simulation of machining processes appears to be an important approach to control and monitor operating cutting parameters. Developing a machining numerical model for predictive purposes, based on a physical understanding, is possible only through proper comprehension of thermomechanical phenomena occurring during the tool–workpiece interaction [4]. Imperfect knowledge of certain physical effects on this interaction constitutes a real obstacle to the development of a robust numerical simulation of processes. From a numerical point of view, the modelling of machining is referring to the theory of finite transformation considering both thermomechanical coupling and also tribological phenomena during the dynamic cutting process. According to the literature, three approaches can be adopted in machining modelling. Definitions and boundaries of these approaches are not always in agreement within the scientific community:

- macroscopic approach: dealing with the overall behaviour of the machining system and what it can induce at the tool–workpiece interaction (vibration, chatter, stability, etc., order of metric scale ∼30–300 mm),
- mesoscopic approach: treating tool–workpiece interaction at the level of chip formation (order of metric scale ∼0.3–30 mm),
- microscopic approach: treating the consequences of machining in terms of phase transformations in the machined material (order of metric scale ∼3–300 μm).

In the following, we will be primarily focus on the mesoscopic scale. In this context, it should be noted some work researches to optimise cutting through the analysis of the chip formation [5]. Certainly, the chip is a process waste. Nevertheless, its genesis allows a detailed physical understanding of the cutting process and its optimization. It is an efficiency indicator of objective information as it will be discussed later.

Despite the large volume of studies of chip formation discussed for more than one century [6] where Henri Tresca [7] was the first to analyse chip formation and to give a "prospective opinion" about the importance of "the investigation of the cutting process" to better design tools, many drawbacks persist up to now concerning the understanding of the tool–workpiece interaction. The difficulties we are faced with in the optimising of machining processes are also due to industrial feedbacks, in close relationship with some new developments and improvements. To illustrate these purposes, three examples should to be mentioned. The first concerns the improvement of mechanical behaviour of certain materials to be processed over the past twenty years. This can be presented by increasing such material characteristics by the introduction of heat treatment methodologies or the addition of chemical additives and inclusions. This strongly guides the process optimization to the development of new methodologies of analysis and characterisation.

The second example concerns the finishing of steels with hardness greater than 55 HRC (or about 600 HV or 570 HB or $R_m = 900$ MPa). Indeed, these materials are now increasingly finished in hard turning and not with grinding process. This cutting operation is usually performed with a polycrystalline cubic boron nitride (CBN) insert having a nose radius sufficiently large, and a very rigid machine tool. To understand this machining operation and monitor the industrial production, it is important to identify the type of serrated chip involved and qualify the resulting surface texture. Moreover, in hard turning, many studies of tool wear evolution, as a function of the cutting parameters, are currently the subject of industrial research and development. Consequently, these potentially lead to new and more efficient CBN grades.

The third example offers some implementation difficulties and scientific understanding about the chip formation in the High Speed Machining (HSM) increasingly used in many industrial sectors [8]. This is the result of the appearance of a large range of means such as new design of machine tools, control systems, scheduling systems, monitoring systems, etc. The transition to high speed is a global action always complex, involving all aspects of production. HSM often brings significant advantages in terms of productivity, manufacturing cost, and product quality, but it is also generating various constraints. The cost of the equipment and the hazards associated with high rotational speeds and feeds implies that the development of HSM has to be avoided by trial and error. Programming trajectories, the choice of tools and cutting conditions must be flawless. Some incidents, shock, vibration or tools that are already hindering at conventional speeds have catastrophic proportions at high speeds. New methodologies and approaches have to be proposed for improving HSM processes by adopting, for example, robust numerical simulations to verify some choices and avoid abnormal situations.

In general, it can be noted that numerical simulations give more specific results, for example about the strain field distribution, stress and/or temperature within the machined material and tool, etc. The earliest numerical modelling of cutting is a purely mechanical-based Lagrangian description without coupling with temperature. Since the 1990s, different models based on an Eulerian description appeared. With this approach, problems due to mesh distortion or material separation at tool-tip are no longer concerned. The major drawback of the Eulerian approach is the difficulty of the treatment of model-free surfaces. The final geometry must be known in advance or model must include an updating algorithm of the free surfaces during calculation. It is noteworthy that the development of the arbitrary Lagrangian–Eulerian method (ALE) offers the opportunity to combine the advantages of both conventional initial descriptions. The dissociation between the evolution of the mesh and matter simultaneously allows overcoming the distortions without considering a material separation criterion.

The machining modelling studies include several aspects depending on the fineness of the adopted scale. In the present contribution, it is emphasised to study chip formation during cutting operations. To study the mechanism of chip segmentation, the effect of cutting conditions on the evolution of cutting forces is treated. Also, an investigation on chip strain localisation is carried out. Numerical studies treating different methodologies to simulate chip formation based on the theory of strain gradient plasticity is discussed. Moreover, the effect of machining system stiffness on the chip segmentation is presented. The chip study is not an ultimate goal to reach among this paper because it is the irrecoverable part, the "waste" in machining, but it is an efficient indicator to bring more physical comprehension of the cutting process.

2. Chip formation and morphology: case of hard turning

2.1. Mechanism of chip segmentation

For hard turning, most chips have *waved geometry*, also known as *sawtooth* or *segmented* chips. This morphology is interesting from a scientific point of view because its genesis is generated dynamically during the machining operation. For a thermomechanical understanding of the segmented chip formation and to draw conclusions on the interaction of the tool with the material being machined, it seems essential to explain how this segmented chip is formed. The research work in

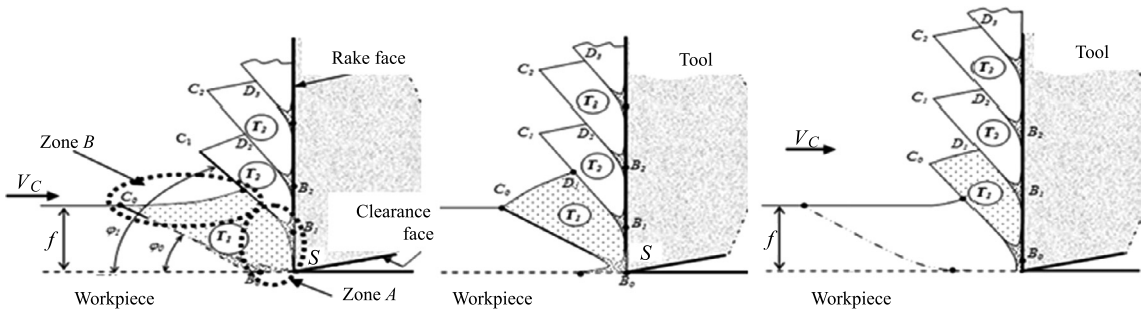

a) T_1 is jammed between the rake face and (SC_0)

b) T_1 tends to slide towards the free surface (C_0D_0)

c) T_1 slides and takes the form of a sawtooth

Fig. 1. Chip genesis [9,10].

Table 1
Used insert geometries and cutting conditions.

Coated carbide inserts CNMA 12 04 04 AC700G Sumitomo Electric (ISO K15, TiCN-Al203) [10]				
Entering angle: χ_r 95°	Rake angle: γ_o −6°	Clearance angle: α_o 6°	Inclination angle: λ −6°	Insert radius: r_ϵ 0.4 mm
Conditions de coupe				
Cutting speed ($60 \leq V_C \leq 120$) m/min		Feed rate ($0.2 \leq f \leq 0.47$) mm/rev		Cutting depth ($a_p = 1$ mm)

this context, concerned turning hardened steel to 47 HRC (case of 35NiCrMo16 (UNI), named also AISI 4340). To do this, an experimental study was conducted for different cutting speeds and feed rates. It is based on both:

- gathering at high-frequency cutting force signals,
- carrying out measures of the onset wavelength primary shear bands and chip segmentation frequency.

For reasons of convenience, chip formation has been studied in a plane perpendicular to the cutting edge as shown schematically in Fig. 1. This global mechanism of chip formation is illustrated based on observations summarising the training cycle of a segment or a tooth T_1 [9]. The initial stage is characterised by compression and bulging of the new tooth (C0 B0 B1 D1), where two zones are noted A and B. Zone A near the tool tip named "S" and is under high-pressure levels. This place is jammed between the rake face of the tool and the limit (SC0). As the cutting time increases, the jammed material tends to escape to the free side (C0D1) [10]. The stage of the deformation of T_1 may be accompanied by a crack initiated at C0. Thereafter, the metal will be pushed to area B; far away the tool tip. This causes a bump on the free surface (C0D1) and a slip condition of T_1 along a shear plane (direction B*i*C*i*). In this cycle, a large amount of plastic deformation work is converted into heat. This causes the thermal softening phenomenon of material, mainly in the primary deformation zone.

The succession of cycles leads to the formation of the chip sawtooth. Each tooth is bounded by two shear planes of length C_iC_{i+1}, characterising the saw teeth periodicity. This chip segmentation causes a variation of the chip's section. Consequently, this change will certainly have a considerable influence on the variation of cutting forces and chip evacuation speed. Although there are many significant papers and different methodologies adopted for the study of chip formation, it can be noted that there are quite a few results on the effects on the variation of the components of cutting force [11] and on the quality of the machined surfaces, speciality the surface roughness and the residual stress distribution. This is especially important in hard turning where it is tried industrially to get mechanical parts with quality close to that derived from the grinding process.

2.2. Chip shear band formation frequency

Measuring equipment A series of tests was conducted on a GALLIC universal machine-tool (20 kW). Straight turning operation was carried-out on workpiece (AISI4340, heat treated at 47HRC) with an external diameter $D_{wp} = 70$ mm [10]. The machining was carried-out with coated carbide inserts (Table 1).

The average values of the cutting force and its amplitude variations were recorded by a chain of measurement consisting of a dynamometer Kistler Type 9257B, a Kistler charge amplifier Type 5015, and a map of acquiring high-frequency Ni-4472 of National Instrument data.

The frequency representation of the gathered temporal signal of the cutting force is elaborated via a Fast Fourier Transform (FFT) signal presented in Fig. 2a. The latter shows the presence of an important peak at frequency of $F_{Seg\text{-}signal} = 8262$ Hz, with higher power level. This is clearly the most powerful frequency identified.

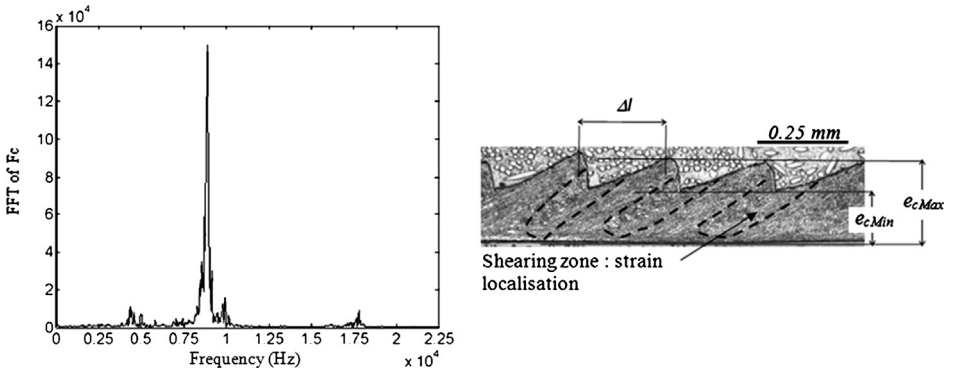

Fig. 2. a) Cutting force signal ($V_C = 80$ m/min, $f = 0.125$ mm/rev, $a_p = 1.65$ mm), b) segmented chip, AISI 4340 (47 HRC), ($V_C = 120$ m/min, $f = 0.2$ mm/tr, $a_p = 1$ mm). (NB: This image has been processed by changing contrast and brightness.) [10]

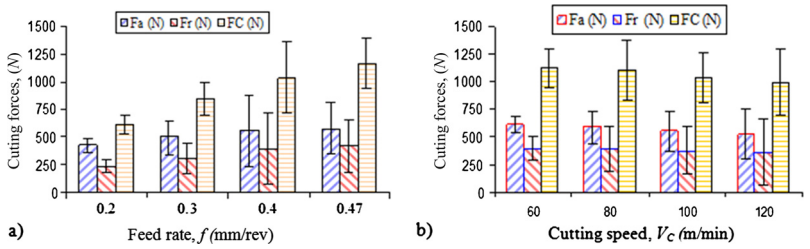

Fig. 3. Evolution of cutting forces a) for $V_C = 100$ m/min, b) for $f = 0.4$ mm/rev.

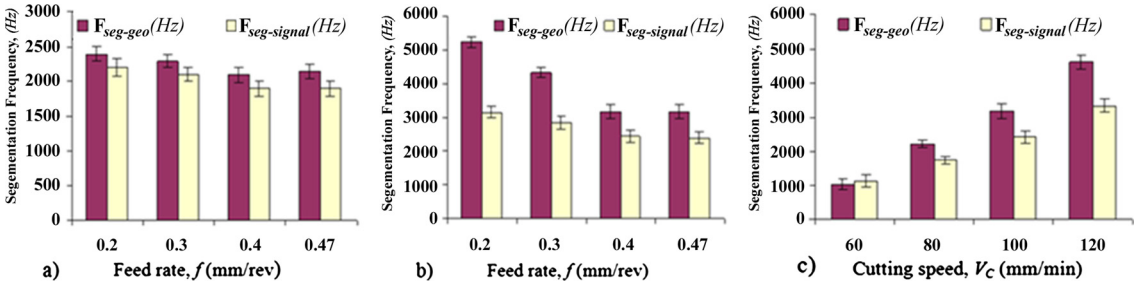

Fig. 4. Chip segmentation frequency according to f at a) $V_C = 80$ m/min, b) $V_C = 100$ m/min, and V_C at c) $f = 0.40$ mm/rev.

Also, geometric measurements were performed on the chip by considering an average speed of the chip evacuation on the tool rake face. This speed can be calculated by assuming that the cut material is conserved and incompressible during the cutting operation. Moreover, the measured distance between two consecutive segments allows the calculation of the segmentation frequency noted here $F_{\text{Seg-geom}}$.

Effect of cutting conditions on cutting forces Fig. 2b shows a segmented chip obtained at $V_C = 120$ m/min and $f = 0.2$ mm/rev. The presence of deformation zones is due to a localized shearing phenomenon. The periodicity of this deformation causes the sawtooth-shaped chip. Therefore, the chip evacuation speed is not constant over time. These periodic variations can be correlated with variations in cutting forces during their measurements.

Fig. 3 shows the influence of the feed rate and cutting speed on the evolution of the axial F_a, radial F_r, and tangential F_c cutting forces. It can be noticed that the feed rate tends to affect highly the cutting forces when compared to the effect of the cutting speed, which tends to slightly decrease the cutting forces. It is also noted that the tangential cutting force, F_c, is the most important one, followed by the axial force, F_a (along the feed rate), and the radial one F_r.

Chip segmentation frequency evolutions Fig. 4 shows the influence of f on the frequencies mentioned above. During the cutting process, the chip segmentation frequency, $F_{\text{Seg-geom}}$, decreases with f (Fig. 4a). This decrease is even more important when the cutting speed is higher (Fig. 4b). Increasing f or V_C, as already mentioned in the experimental work of Poulachon [11] promotes strain localisation within the chip and sawtooth segments are more clearly formed. Nevertheless, the increase in feed rate (Fig. 4a–b) yields to higher distance of PIC-to-PIC consecutively chip segments, whereas higher cutting speed allows lower distance of PIC-to-PIC ones. Consequently, it can be noted an increase in chip segmentation frequency with V_C

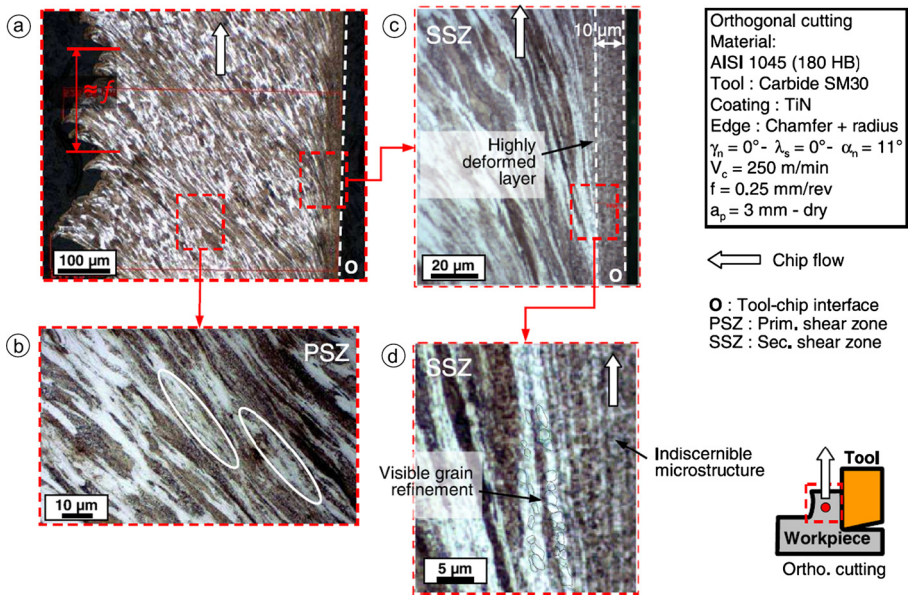

Fig. 5. a) Chip micrographs (AISI 1045) (Nital 2% – 10 s): b–c) highly deformed in PSZ–SSZ, d) fine equiaxed grains [12]. Here the cutting edge radius is $r_\beta = 50$ µm, approximately.

(Fig. 4c). This proves that the chip fragmentation in turning can be, among others, the result of this segmentation phenomenon. Based on plots in Fig. 4, it can be said that the frequency $F_{\text{Seg-signal}}$, characterising the spectrum of the tangential cutting force, is practically equal to the frequency $F_{\text{Seg-geom}}$, calculated from the geometric measure made on the collected chips after machining.

When analysing variations between the frequencies $F_{\text{Seg-signal}}$ and $F_{\text{Seg-geom}}$, it can be observed the existence of a little gap between them. Nevertheless, their tendency regarding cutting conditions remains the same. This little gap is due, among others, to the approximation adopted for the evaluation of the chip evacuation speed needed to calculate the frequency $F_{\text{Seg-geom}}$. The complexity of the phenomena accompanying the sawtooth chip formation can be also at the origin of this gap.

The formation of the chip is accompanied by certain mechanisms such as localized shear which can yield towards a "catastrophic" material behaviour in the chip with an extension of cracks. Other aspects can also affect chip formation and make the chip genesis comprehension more complex. Indeed, it is important to underline that a complete study yielding to the physical understanding of the tool–workpiece interaction have to take into account the thermo-mechanical and thermo-chemical characteristics of the worked material, the tribological conditions of tool–chip contact and the possible interactions between primary and secondary shear zone, etc. Finally, the dynamic behaviour of the whole machining system can influence this process of segmentation as discussed in the following.

Numerical cutting simulation can be complementary to machining experimentation. Indeed, it is financially attractive and can bring fine investigation of the tool–workpiece interaction.

2.3. Investigations on chip strain localisation

The genesis of the chip can be described among others, as it was seen earlier, by cutting forces measurements, segmentation frequencies or its geometrical morphology, etc. Also, it can be underlined that fine chip observations can improve the understanding of the physical mechanisms accompanying its genesis. In particular, one can imagine using metallurgical analysis to investigate the history of the stresses imposed on the material. In this context, instrumented tests [12] in the case of dry orthogonal cutting were carried out on standardised AISI 1045 steel and 42CrMo4 tempered and quenched steel. These steels have different microstructures and mechanical properties. This experimental study was first possible to highlight the differences in behaviour to the cut depending on the operating conditions. The study was focused on the machining forces, heat transfer (flux transmitted to the cutting tool) and on the analysis of chips and cutting tools after use. If the heat flux and the efforts were very similar from one material to another, the differences appear mainly on the morphology of the chip (thickness, segmentation, expansion) and on the faces of tool-material contact zones.

Fig. 5a shows a typical microstructure of the continuous chip of a ductile material AISI 1045. The material is deformed in a relatively homogeneous way without localisation, even if a slight shear band is noticeable. Nevertheless, pseudo segmentation can be found with an average period corresponding to feed rate f with a shear angle about 24 to 26°. Chips collected on 42CrMo4 (Fig. 6a) are almost similar to those obtained in hard turning. Segmentation period appears again substantially

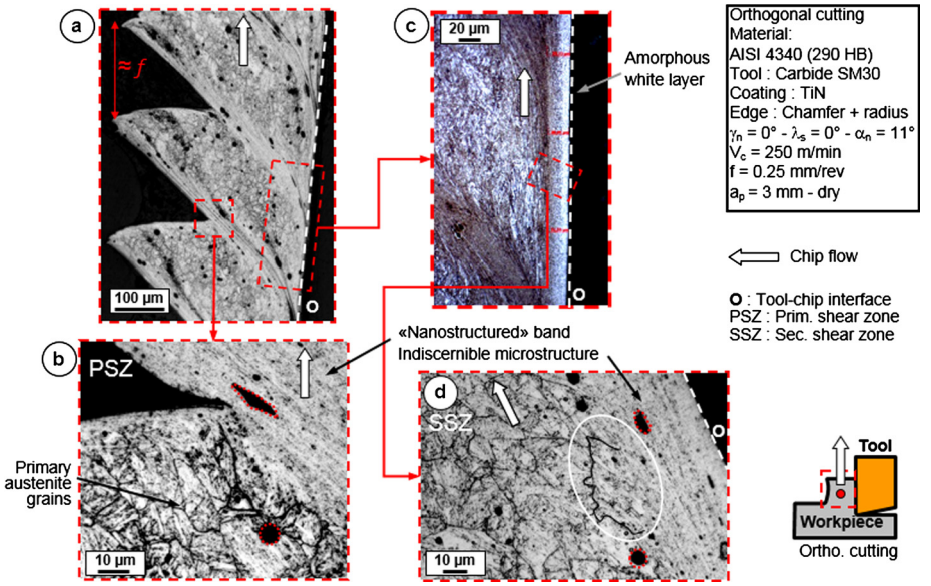

Fig. 6. a) Chip micrographs (42CrMo4) ("Béchet–Beaujard", 70 °C – 2 min et Nital 2% – 5 s): b–d) undeformed microstructure and highly deformed in PSZ–SSZ, c) white layers [12].

equal to the feed rate f as it was cited in the work of [11] in case of the machining of a bearing steel. The shear angle is here most important (28 to 36°).

When observing in detail the two major deformation zones (primary shear zone (PSZ) and secondary shear zone (SSZ)), one can remark that for the AISI 1045 steel, in the (PSZ), the ferrite grains are elongated (Fig. 5b). The areas circled in the "shear band" suggest subdivisions within the very work-hardened grains, the optical analyses do not provide strong support for these findings. Perlite seems meanwhile completely unstructured at this observation level. Fig. 6b illustrates the quite different behaviour of 42CrMo4. Indeed, it is possible to distinguish a less deformed chip segment, limited by two zones characterised by a localized high shear. The chip genesis mode of 42CrMo4 can be described similarly by what it was proposed by many authors in the hard turning such as the work in [13] or the work in [11] in the case of the machining of AISI 52100 (100Cr6). Note the presence of undeformed oxides out of the highly sheared zone and stretched within this area. If little deformed grains turn out quite similar to those of the initial microstructure, it is impossible to discern any structural organisation in the shear band.

The secondary shear zone (SSZ) is fairly clearly in Fig. 6c–d (case of AISI 1045) and Fig. 6c–d (case of 42CrMo4). It is characterised by a high level of deformations caused by intense thermo-mechanical loads generated at the tool–chip interface. In Figs. 5c and 6c, it can be remarked that the surface that was in contact with the tool has a uniform layer. For both material grades, the level of deformation is such that it is impossible to identify the microstructure, even at high magnification. Its thickness varies from 10 to 30 microns depending on the cutting conditions. On 42CrMo4 after a Nital treatment (Fig. 6c), it appears as a white layer.

The imaging of chip structure by Electron Back Scatter Diffraction (*EBSD*) has been exploited [12,13]. It allows us to locally measure the crystallographic orientation and in particular to give access to the distribution of grain boundaries or to the intragranular orientation gradients. This technique has permitted to observe chip microstructural changes (material AISI 1045) operating in the two pre-cited zones ((PSZ) and (SSZ)) (Fig. 7a).

- In (*SSZ*) (Fig. 7b), different zones of deformation can be underlined. Zone I is formed by nanosized grains (very refined grains) very equiaxed (∼ 200 nm) (Fig. 7c). This zone was uniform on optical technique. A second zone (II) can be detected. It is characterised by a mixture of relatively fine and equiaxed grains (∼500 nm) with others very elongated, and a zone having equiaxed grains but of larger diameters (0.3–1 µm).
- In (*PSZ*) (Fig. 7d), it can be observed the presence of the two components, ferrite and pearlite. If it appears rather unstructured in some areas (fracture of the lamellae and dispersed distribution), the ferrite grains with initial size of 10–20 µm are substantially "refined" with a diameter varying between 0.5 to 1 µm.

Based on the pre-cited observations, it can be confirmed that a grain refinement phenomenon can take place under high loadings (nanostructuring). These findings corroborate with those brought by Vandijck [15] when studying the contact problem of pin-disk/copper-steel. Authors had already proved from TEM analysis that the friction has yield to a nanostructured layer with grain sizes even approaching 20 nm. It is interesting to note that on the obtained EBSD map in Fig. 7b, it appears that the intragranular disorientation is almost zero. This indicates a rearrangement of dislocations leading the material to a more stable state, which is at the origin of the recovery and recrystallisation of metals. Finally, note that it is impossible

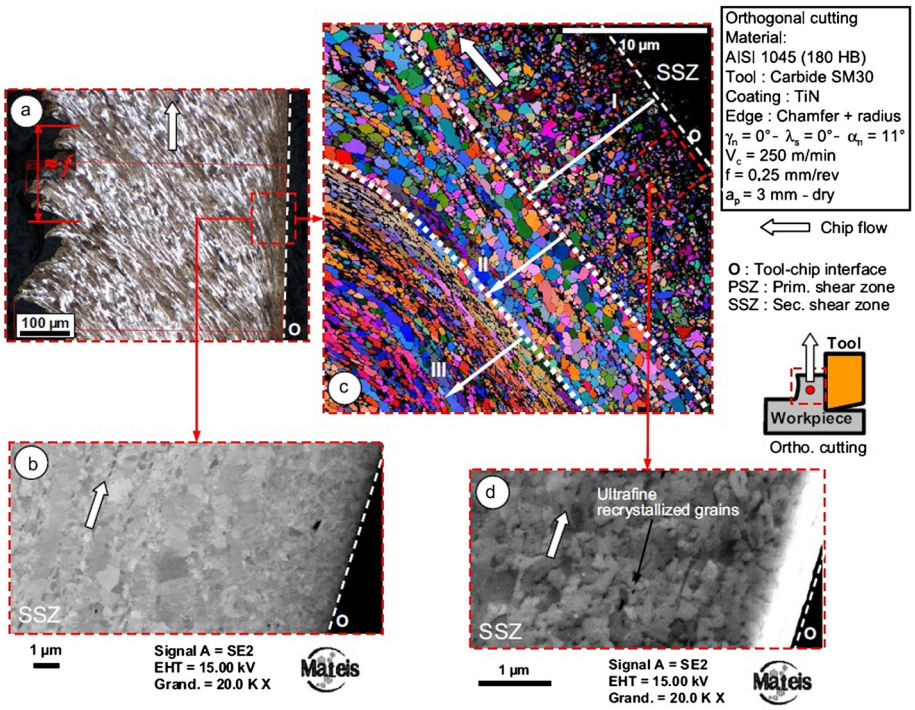

Fig. 7. MEB + EBSD analysis of the deformation zones (chip, AISI 1045) a) optical micrograph, b) EBSD map (Euler angles) SSZ, c) MEB HD (recrystallised structure), d) MEB: SSZ [12,14].

to find any trace of cementite in Fig. 7c–d. If its diffusion to the chip surface seems unproved, one can very well imagine that the iron carbides could dissolve due to high deformations and temperatures levels reached in this zone. The diffusion of carbon atoms has in fact been facilitated by disturbances caused by the dislocations in the crystal lattice.

3. Numerical models for orthogonal cutting simulations

3.1. Numerical methodology for cutting model elaboration

In order to elaborate multi-physical cutting numerical models, many methodologies were adopted in the literature. It is important to underline that numerical modelling of cutting is a complex task due to the diversity of the physical phenomena involved. Indeed, large elastoviscoplastic deformation, severe contact/friction conditions, thermo-mechanical coupling, and chip separation mechanisms have to be included, etc. This complexity is considerable when dealing with chip detachment criteria and considering physical phenomena occurring at cutting edge vicinity characterised by highly localized strains that are not directly observable by means of an experimental procedure.

Among the literature published [16] in the topic of machining modelling based on FE method, it is mentioned that the Lagrangian approach is widely used to model the description movement inside a cutting model. This approach helps to obtain numerical chip morphology near the experimental one. The Lagrangian formulation assumes that the *FE* mesh is attached to the cut material and follows its deformation. This provides simpler schemes to simulate transient processes and discontinuous chip formation. However, element distortion has restricted the analysis to incipient chip formation or machining ductile materials using larger rake angles, and/or low-friction conditions [17] re-distorted [18] re-meshing [19] have been used to minimise the problem.

In Eulerian formulation, the mesh is fixed in space and material flows through the element faces allowing large strains without causing numerical problems. This strategy is not affected by element distortion and allows a steady-state machining to be simulated. However, Eulerian approach does not permit element separation or chip breakage and requires a proper modelling of the convection terms associated with material properties. In addition, such formulations also require the prior knowledge of the chip geometry and chip–tool contact length, thereby restricting the application range.

It should be noted that the development of Arbitrary Eulerian–Lagrangian methods (ALE) offers the opportunity to combine the advantages of both the pre-cited classical descriptions. The dissociation between the evolution of the mesh and the material helps to overcome the distortions and to deprive from a criterion yielding to separating nodes at the tool-tip zone when modelling the chip detachment. This method applies Lagrangian and Eulerian steps sequentially and uses a so-called operator split. The first step assumes that the mesh follows the material flow, in which a Lagrangian problem is solved for displacements. Subsequently, the reference system is moved (the mesh is repositioned) and an advection problem (Eulerian

step) is solved for velocities. Despite the fact that ALE methods reduce the element distortion problem typical of Lagrangian approaches, a careful numerical treatment of the advection terms is required. More elaborate discussion on the use of ALE formulations in modelling metal machining are presented in [20–22].

In the present paper, a Lagrangian approach methodology was adopted for the development of different cutting models. These methodologies were accomplished in several major steps.

The first step involves the elaboration of a numerical 2*D* cutting model. This has helped to adopt some details for the development of other numerical models. These details concern the strategies of mesh discretisation, cut material behaviour, material damage, boundary conditions, etc.

In the second step, the model was adapted to the case of the modelling of a 2D plane of down-cut peripheral milling with zero helix angle. In this model, the intended material to be removed has a half-moon shape. In this model adaptation, the chip has a continuously variable thickness, which is approaching zero, theoretically. Consequently, the well-known size effect in micromechanics has to be considered when the macro–micro passage through the influence of work hardening caused by the material strain rate effect. The well-known experimental phenomenon consisting to the exponential increase in the specific cutting energy with the chip decreasing thickness has been highlighted.

In order to catch the size effect during the modelling of the down-cut peripheral milling and provide a physical understanding of the tool machining, the behaviour model "Johnson–Cook" was modified by an approach based on the second gradient of displacement (*SGD*) by developing in ABAQUS®/Explicit a user routine VUMAT.

In addition to size effect which can be considered during chip thickness variation in down-cut peripheral milling, the dynamic behaviour of the machining system can affect considerably chip genesis. In this framework, a multi-scale model named "hybrid dynamic cutting model" (HDC-model) that combines the equivalent rigidity of a high speed milling machine (tool, tool holder, spindle, etc.) (macroscopic level) with the process of chip formation (mesoscopic level) is presented. The pre-cited models were validated experimentally in the case of the machining aluminium alloy A2014. Moreover, previous elaborated methodologies have allowed establishing mesoscopic cutting models taking into account the consideration of the variation of the limiting shear stress $\tau_{\lim}$ regarding the variation of both friction coefficient and temperature. For that, a user routine VFRIC was developed in ABAQUS®/Explicit.

3.2. Constitutive material models and chip separation technique

The material constitutive model is usually required for cutting simulations. It permits to associate material flow stress with strain, strain rate, and temperature.

Various numerical studies in the case of machining have been performed using a wide range of constitutive models for the concerned workpiece, such as rigid plastic [23], elastoviscoplastic [24] materials, etc. One of the most popular material formulation (elastothermoviscoplastic) adopted is the one proposed by Johnson and Cook [25]. It provides a practice description of metal material behaviour undertaking large strains, high strain rates and temperature-dependent viscoplasticity. This model is presented by the following expression of the equivalent plastic flow stress:

$$\bar{\sigma}_{JC} = \left[A + B \times \left(\bar{\varepsilon}^{p}\right)^{n}\right] \times \left[1 + C \times \ln\left(\dot{\bar{\varepsilon}}^{p}/\dot{\bar{\varepsilon}}_{0}^{p}\right)\right] \times \left[1 - \left(\frac{T - T_0}{T_{\mathrm{m}} - T_0}\right)^{m}\right] \tag{1}$$

Several modelling studies have shown the effectiveness of this material flow stress model [26,27]. Later, Calamaz et al. [28] developed a new material constitutive law, which takes into account the influence of strain, strain rate, and temperature on the flow stress and also introduces a strain softening effect. Similar to Calamaz et al. [28], Sima and Ozel [29] also improved the Johnson–Cook model by considering the temperature-dependent flow softening, in which the flow-softening phenomenon, strain hardening, and thermal softening effects and their interactions are coupled.

The critical algorithms which can be evoked during FE-based simulation (for the Lagrangian formulations) of the cutting process are specified as the technique of chip separation criteria, which can be classified into the following three categories.

- The node separation technique (named also debonding method): is a geometry-based approach [30,31]. A predefined parting line is used to separate the chip layer from the workpiece. At each point on the parting line, two nodes are tied together initially and share the same degree of freedom. When the tool approached the tied pair of nodes, they separate based on a pre-specified criterion which is met. Another commonly used criterion is the tool node distance, critical effective stress, and critical effective plastic strain.
- The element deletion technique [32]: is also a geometry-based approach in which the chip layer is predefined by a sacrificial element zone positioned at the bottom of the chip. When the tool approaches a sacrificial element, the latter will be deleted. This will occur based on a given criterion such as critical effective plastic strain or critical energy density.
- The mechanical fracture approach: the use of the latter criterion to determine chip separation is controversial since there is no consensus in the literature on whether chip formation indeed occurs by fracture or not. However, many researchers are using this technique and promising results are obtained [33]. Lately, Subbiah and Melkote [34] have shown that fracture occurs in the tool edge vicinity through the experimental study for machining of the aluminium alloy A2024.

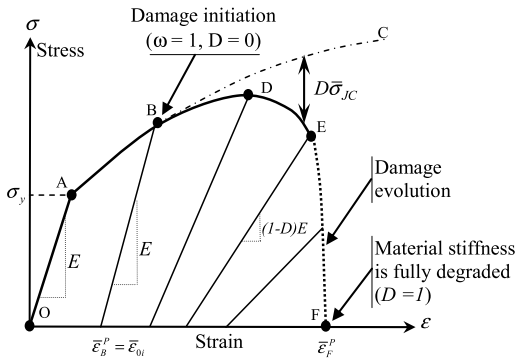

Fig. 8. Typical uniaxial stress–strain in the case of a ductile metal.

Developed models are based on the evolution of a ductile fracture criterion. This implies the possibility of a localisation problem related to the adoption of damage laws when using too dense meshes. In fact, behaviour laws, when they have a softening character, induce sensitivity results regarding the mesh fineness. In order to overcome the problem of mesh sensitivity many "localisation limiters", also called "regularisation technique", can be used to enrich the mechanical description of the continuum. This helps to describe inhomogeneous deformation states and avoid mesh sensitivity during the softening phase. For this, the commonly used technique is to consider stresses in a material point no longer described in a local way, but they have to take into account a characteristic length or an internal time reflecting the interaction of a material point with its neighbours. This keeps in memory, at the macroscopic level, information on the material microscopic behaviour (effect length, maximum evolution speed, etc.). Thus many regularisation techniques, among others, can be used such as strain gradient models, delayed effect models and non-local models [35]. The latter technique was used in the next proposed cutting models. Indeed an internal length was introduced in the used damage model based on Hillerborg's fracture energy [36] as it will be next discussed.

In order to simulate the chip formation, an energetic criterion [33] presented by a failure damage model can be exploited for modelling the cutting process. In this case, the principle of material behaviour evolution can be illustrated via a typical uniaxial stress–strain curve in the case of a ductile metal, as shown in Fig. 8.

Indeed, the response of the latter is initially linear elastic (O–A) followed by plastic yielding with strain hardening (A–B), wherein the curve ABC is the undamaged stress–strain response (Fig. 8). The effect of the damage on the behaviour becomes sensitive at point B, leading to a progressive decrease in the tangent modulus (or hardening modulus). The point D corresponding to the maximum stress is given by the fact that the hardening modulus reaches zero value for a significant value of the ductile damage ($0.3 \leq D \leq 0.7$ depending on the material type). The point E corresponds to the observed fracture while the point F indicates the theoretical final fracture. Clearly the progressive decrease of Young's modulus starts just after the point B as indicated in the figure given below. The deformation during B–F is localized in a neck region of the specimen. Point B identifies the material state at the onset of damage, which is referred to as the damage initiation criterion. Beyond this point, the stress strain response (B–F) is governed by the evolution of stiffness degradation in the region of strain localisation. The chip formation, by ductile failure phenomenon, occurs in two steps. The first step concerns the damage initiation whereas the second one concerns damage evolution based on the fracture energy approach.

Damage initiation The Johnson–Cook shear failure model was used as a damage initiation criterion. It contains five failure parameters, which must be specified ($D_1 \ldots D_5$).

$$\bar{\varepsilon}_{0i}\left[D_1 + D_2 \exp\left(D_3 \frac{P}{\bar{\sigma}_{JC}}\right)\right] \times \left[1 + D_4 \ln\left(\dot{\bar{\varepsilon}}^p / \dot{\bar{\varepsilon}}_0^p\right)\right] \times \left[1 + D_5\left(\frac{T - T_0}{T_f - T_0}\right)\right] \tag{2}$$

The variables $D_1 \ldots D_5$ represent the material parameters of the damage law. The other parameters of Eq. (2) have the same meaning as for the flow law of Johnson–Cook (Eq. (1)). The term $[D_1 + D_2 \exp(D_3 \frac{P}{\bar{\sigma}_{JC}})]$ reflects the decrease of the equivalent strain at fracture when the hydrostatic pressure P increases. It can be recalled that most of the studies concerning cutting modelling use cavity growth and coalescence theory of damage to manage the ductile cutting simulation on the basis of the work of Rice and Tracey [37].

The damage in a given finite element is initiated when a scalar damage parameter ω exceeds 1. This parameter is based on a cumulative law defined as:

$$\omega = \sum_{j=1}^{n} \left(\frac{\Delta \bar{\varepsilon}^p}{\bar{\varepsilon}_{0i}}\right)_j \tag{3}$$

where $\Delta \bar{\varepsilon}^p$ is the increment of equivalent plastic strain during an increment of loading, j, in each integration point.

Based on the pre-cited equation, the stress triaxiality ($\frac{P}{\bar{\sigma}_{JC}}$), strain rate effects and temperature can induce damage initiation and so the propensity for fracture increase [38].

Damage evolution The Hillerborg's fracture energy [36] was introduced to model damage evolution. There are mainly two reasons for introducing the Hillerborg's fracture energy. Firstly, it can be used to control the material degradation after the damage initiates, which makes the failure process more stable. Secondly, it is interesting to capture high strain localisation during chip segmentation even for relatively large size element.

It is noted that when ductile material damage occurs, the stress–strain relationship no longer accurately represents the material behaviour. Continuing to use the stress–strain relation introduces a strong mesh dependency based on strain localisation, such that the energy dissipated decreases, as the mesh is smaller. Hillerborg's fracture energy proposal [36,39] allows reducing mesh dependency by creating a stress–displacement response after damage initiation. Hillerborg defines the energy required to open a unit area of crack G_{f}, as a material parameter. With this approach, the softening response after damage initiation is characterised by a stress–displacement response rather than a stress–strain response. The fracture energy is then given as:

$$G_f = \int_{\bar{\varepsilon}_{\mathrm{B}}^{\mathrm{p}}}^{\bar{\varepsilon}_{\mathrm{F}}^{\mathrm{p}}} L\bar{\sigma}\,\mathrm{d}\bar{\varepsilon}^{p} = \int_{0}^{\bar{u}_{F}^{\mathrm{p}}} \bar{\sigma}\,\mathrm{d}\bar{u}^{\mathrm{p}} \tag{4}$$

This expression of G_{f} introduces the definition of the equivalent plastic displacement $\bar{u}^{\mathrm{p}}$, as the fracture work conjugate of the yield stress after the onset of damage (work per unit area of the crack). The implementation of this stress–displacement concept in a finite element model requires the definition of a characteristic length, L, is the square root of the integration point element area based on a plane strain element CPE4RT. The length L is based on the element geometry, which is in the present study a planar element (CPERT). This definition of the characteristic length L is used because the direction in which fracture occurs is not known in advance. Therefore, elements with large aspect ratios will have rather different behaviours depending on the direction in which they crack: some mesh sensitivity remains because of this effect, and elements that have aspect ratio close to unity are recommended [39].

Where $\bar{\varepsilon}_{B}^{p}$ and $\bar{\varepsilon}_{F}^{p}$ are the equivalent plastic strain at points B and F. $\bar{\sigma}$ is the equivalent plastic stress.

The scalar stiffness degradation for the linear damage process is given by:

$$D = \frac{\int_{\bar{\varepsilon}_{\mathrm{B}}^{\mathrm{p}}}^{\bar{\varepsilon}^{\mathrm{p}}} \bar{\sigma} L\mathrm{d}\bar{\varepsilon}^{p}}{G_{\mathrm{f}}} = \frac{\int_{0}^{\bar{u}^{\mathrm{p}}} \bar{\sigma}\,\mathrm{d}\bar{u}^{\mathrm{p}}}{G_{\mathrm{f}}} \tag{5}$$

Whereas an exponential damage parameter can evolves according to:

$$D = 1 - \exp\left(-\int_{0}^{\bar{u}^{\mathrm{p}}} \frac{\bar{\sigma}}{G_{\mathrm{f}}}\mathrm{d}\bar{u}^{\mathrm{p}}\right) \tag{6}$$

The formulation of the model ensures that the energy dissipated during the damage evolution process is equal to G_{f}. In theory, the damage variable D reaches a value of one only asymptotically at an infinite equivalent plastic displacement. In ABAQUS®/Explicit software, the overall damage variable D never equals to its maximum value (one) and is enforced to be less than or equal to 0.99 when the dissipated energy reaches a value of G_{f}. This ensures that the elements will remain active in the simulation, with a residual stiffness of at least 1% of original stiffness [39].

At any given time during the analysis the plastic equivalent stresses in the material is given by:

$$\sigma = (1 - D)\tilde{\sigma} \tag{7}$$

where $\tilde{\sigma}$ is the effective (or undamaged) stress computed in the current increment. It represents stresses that would exist in the material without damage.

Meshing Four node bilinear-quadrilateral continuum elements referenced as CPE4RT in ABAQUS® can be used for a coupled temperature displacement calculation, in which both displacement and temperature are the nodal variables. These elements have also been tested by several researchers ([22,33,40] and [41]).

CPE4RT are solid elements used for complex nonlinear analysis involving contact, plasticity and large deformations. Nevertheless, these linearly reduced–integration elements under certain loading conditions can experience a pattern of non-physical deformations, called hourglassing. To reduce its effects and to get physical results, either a very fine mesh should be defined and/or artificial damping and/or stiffness must be applied. But there is a limit on refining the mesh; the smaller the element length, the smaller the time step, and analysis will end very costly. Simultaneously, a very fine mesh can lead to strain localisation [17]. For CPE4RT elements, ABAQUS® proposes two types of hourglass treatment approaches:

- the "combined stiffness and damping" method, which is based on the combination of stiffness, acting to maintain nominal resistance throughout the simulation, and damping, generating additional resistance under dynamic loading conditions,
- the "relax stiffness" method, which generates more resistance to hourglass forces early in the analysis step where sudden dynamic is more probable.

Barge et al. [17] have performed a sensitivity analysis for these two approaches according to different mesh densities. They have emphasised on the consistent use of hourglass treatment for physical results. They have concluded that "relax stiffness" is the most efficient method to prevent hourglass modes since its influence on the results is less dependent on the mesh density. For that, the present study therefore incorporates "relax stiffness" approach to minimise the hourglass.

Whatever the type of elements, mesh density plays a vital role in getting physical results from a FEM-based analysis, and it is usually defined on the nature of the problem. Indeed, coarse mesh is sufficient for steady-state elastic problems, while complex plasticity problems leading to damage and crack require the finest mesh to capture localized phenomena. However, a very fine mesh keeps its limitations, as it was said previously.

In the literature dealing with FEM cutting simulation, there is no defined criterion for an optimised mesh density. Barge et al. [17] have shown in their numerical work that the coarser the meshes, the higher are the cutting force oscillations. Otherwise, refined meshes lead to a flattened cutting force curve.

Friction and heat generation Another important feature of the cutting simulation is the consideration of the heat generation due to the simultaneous phenomena of inelastic deformation and friction. This in turn changes the material properties. Therefore, it is necessary to capture the stress, strain and temperature simultaneously with thermomechanical modelling when the material is being removed. So, a coupled temperature–displacement analysis has to be performed.

Nevertheless, some studies have generated physical results with adiabatic hypothesis [41,42]. The solution of the temperature field equation for heat conduction is not required when this assumption is made, but this approximation can only be safely adopted for low-diffusivity materials in high-speed processes. The temperature increase is calculated directly at the material integration points according to the adiabatic thermal balance. If cooling at room temperature is needed in order to evaluate residual stresses inside the workpiece, it is not advisable to adopt this simplification [15]. If such numerical model assumes that the working condition implies adiabatic assumption (for example at a given cutting speed), this is probably not true. Indeed, a calculation based on the criterion developed by Recht [43] or that given by Frost and Ashby [44] should to be checked to see whether conditions are in fact adiabatic or not.

Certainly, for specific cutting parameters both inelastic heating and conduction of the heat are important. So, a coupled temperature–displacement analysis must be included, as it is adopted in the present work.

Also, friction between chip and tool constitutes one of the most important and complex aspects of machining process. It potentially can determine, not only the tool wear and the quality of the machined surface, but also the structural loads and the needed power to remove a certain volume of metal.

The temperature independent, stick-slip friction model, which has been developed by Zorev [45], is one of the most commonly used approximations to frictional contact between chip and tool (Eq. (8)). Zorev advocated the existence of two distinct chip/tool contact regions: near the tool tip, shear stresses τ_f are assumed to be equal to the shear strength of the material being machined, τ_Y, whereas, in the sliding region, the frictional stress is proportional to the normal stress, σ_n.

$$\tau_f = \begin{cases} \tau_Y, & 0 \le \ell \le L_C(\mu\sigma_n \ge \tau_Y) \rightarrow \text{stick} \\ \mu\sigma_n, & \ell > L_C(\mu\sigma_n < \tau_Y) \rightarrow \text{slide} \end{cases} \tag{8}$$

where μ is commonly associated with Coulomb's friction coefficient and l_c is the contact length characterising a transitional contact zone, assumed to be known in advance in most cases. Similar approaches have been applied to simulate machining processes. For example, defining an average friction coefficient over the rake face, separate coefficients for each region, different length for the sticking region, or even neglecting altogether the low stress variation of shear and normal stresses and simply assuming $\tau_f = m\tau_Y (m < 1)$ along the rake face [46].

4. Simulation examples of chip formation and its morphology

4.1. Case of straight turning

In the following, a method consisting in elaborating an orthogonal cutting model is presented. Cutting is investigated under dry conditions.

In this section, some recent modelling methodologies dealing with the physics of chip detachment are presented. The corresponding numerical results are discussed, analysed and compared with experimentation. To bring physical comprehension of the chip formation and its sawtooth morphology ABAQUS software in its explicit approach was exploited. 2-D cutting, commonly known as orthogonal cutting, was considered.

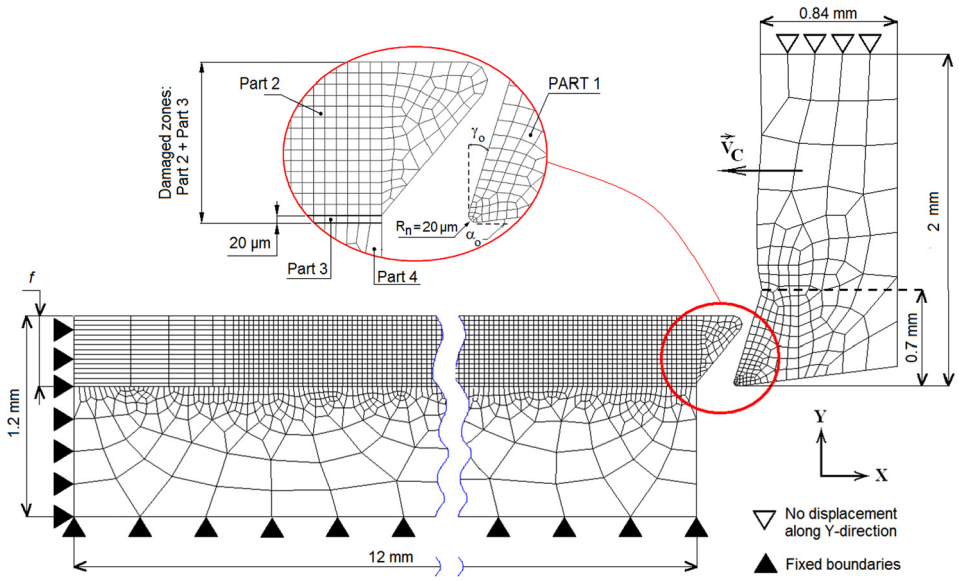

Fig. 9. Grid model and boundary conditions [33].

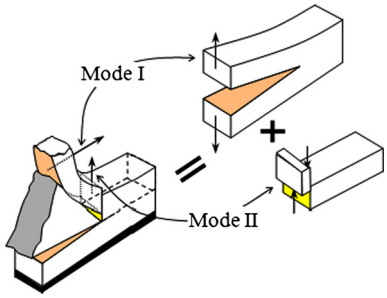

Fig. 10. Orthogonal cutting model of chip formation under mixed fracture modes according to [33]: occurrence of chip detachment (mode I) and its segmentation (mode II).

Fig. 9 shows a schematic representation of the studied model. Quadrilateral continuum elements CPE4RT were used for a coupled temperature–displacement calculation, in which both displacements and temperatures are the nodal variables. It is supposed that the value of feed rate f is lower than that of cutting depth a_p. Consequently, a plane strain assumption for building the cutting model was considered. A contact surface pair was defined between the tool and the workpiece. It consists of two surfaces expected to come into contact during the tool–workpiece interaction. These contact surfaces were designated by the master and slave ones. ABAQUS®/Explicit uses a faceted geometry defined by the finite element mesh as the surface of contact. The interaction between contacting bodies was defined by assigning a contact property model based on Coulomb's friction law.

To optimise contact management during simulation, a multi-part model (Fig. 9) was developed. It was comprised of four parts: the tool (1), the chip (2), the tool-tip passage zone (3), which is a narrower band, and the workpiece support (4). A chamfer was designed on part 2 to avoid distortion problems at the beginning of calculation [33]. The assembly of the various parts, numbered 2, 3 and 4, was carried out by setting a constraint type joining (Tie constraint). The centre of tool tip was placed exactly at the middle height of part 3. The tool geometry is exactly the same as that used in the experimentation and defined in Fig. 8 (cross-section B–B). The tool face angles are: entering angle $\kappa_r = 90°$, rake angle $\gamma_o = 17.5°$ and flank (or clearance) angle $\alpha_o = 7°$. In the case of orthogonal cutting conditions, the feed rate f corresponds to the uncut chip thickness (UCT).

It is underlined also that in this study, the fracture energy G_f is provided as an input material parameter and theoretically is a function of fracture toughness K_C, Young's modulus E and Poisson's ratio ν. Also, it is important to recognise that the fracture toughness parameter K_C takes different values when measured under plane stress and plane strain. Based on fracture mechanics [36], it can be assumed that in the case of the orthogonal cutting process, the two fracture modes (modes I and II) can coexist (Fig. 10). Mode I is a tensile mode (opening mode normal to the fracture plane) and concerns part 3 defined in Fig. 9, whereas mode II is a shearing one (sliding mode acting parallel to the plane of the fracture) and concerns part 2. Consequently, G_f is given in the case of plane strain by Eq. (9). Two different values of fracture energy

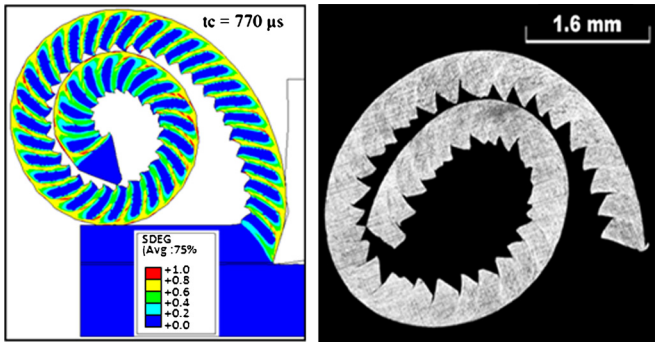

Fig. 11. Computed damage evolution and experimental chip ($f = 0.4$ mm/rev, $V_C = 800$ m/min).

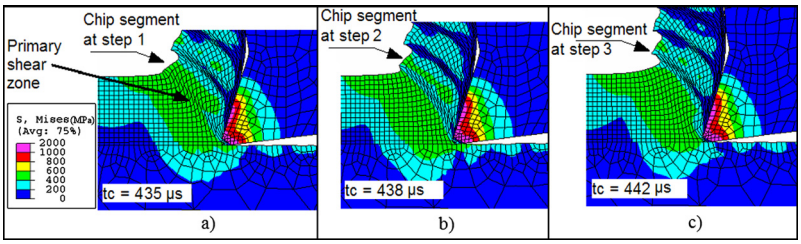

Fig. 12. Distribution of von Mises equivalent stresses during permanent cutting regime ($f = 0.4$ mm/rev and $V_C = 800$ m/min) [33].

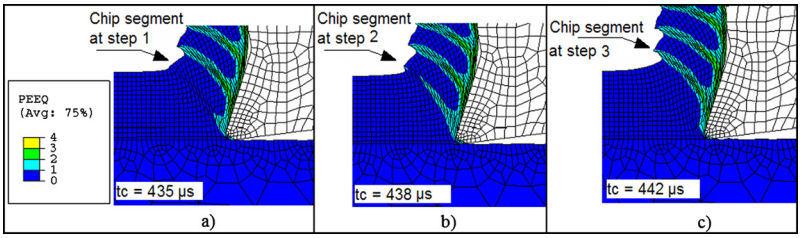

Fig. 13. Distribution of plastic equivalent strain during permanent cutting regime ($f = 0.4$ mm/rev and $V_C = 800$ m/min) [33].

were used as input data in ABAQUS®/Explicit: $(G_f)_I$ for part 3 and $(G_f)_{II}$ for part 2. The subscripts I and II arise because of the different ways of loading. They refer to loading via mode I and mode II, respectively.

$$(G_f)_{I,II} = \left(\frac{1-\nu^2}{E}\right)\left(K_C^2\right)_{I,II} \text{ (plane strain)} \tag{9}$$

In this study, the case of orthogonal cutting of aluminium alloy A2024 is presented. This alloy is widely used in the aerospace industry thanks to its good mechanical properties associated with low density. It is an aluminium alloy of the 2000 series (named also copper series). Its physical parameters, Johnson–Cook law behaviour, Johnson–Cook ductile fracture, and fracture toughness are summarised in [33].

The present section deals with the numerical results obtained during the cutting simulation of an aluminium alloy A2024. A comparison between chip morphology, segmentation, and fragmentation obtained experimentally and numerically is presented. Moreover, the evolution of the cutting force is treated according to cutting speed variations. Finally, the physical mechanisms governing chip tooth shape genesis are studied.

Fig. 11 shows the distribution of the material degradation stiffness (named also damage D) for a complete chip formation for a cutting speed $V_C = 800$ m/min and $f = 0.4$ mm/rev. One can remark that this damage is localized mainly in the shearing zones and in the locations related to tool–workpiece interaction. The inner zone of the chip obtained numerically shows narrower segments, especially in the zones where the chip presents small curvature radii. This result is qualitatively similar to that obtained experimentally. Therefore, as the chip is even rolled up, the segments are closed again.

In order to improve the comprehension of chip genesis, attention is focused on the steps characterising the formation of one chip segment. Figs. 12, 13, and 14 give the distributions of the equivalent von Mises plastic stresses, of the temperature and the equivalent plastic strain during a chip segment's genesis, respectively. In Fig. 12, an increase in equivalent von Mises plastic stresses is to be noted in the primary shear zone, with a decrease in stresses near the tool tip due to a loss in material stiffness. Consequently, the equivalent plastic strain (Fig. 13) and temperature (Fig. 14) increase near the tool tip and evolve towards the chip free side. The damage occurring near the tool tip will extend in a second stage. So, the

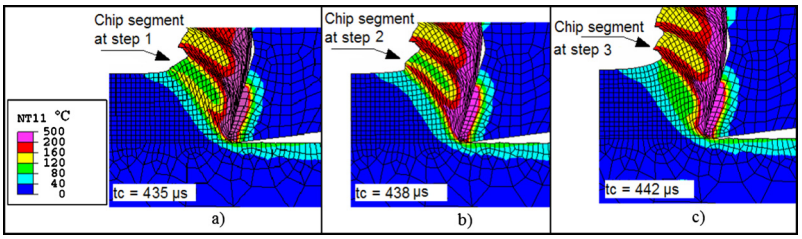

Fig. 14. Distribution of temperature during permanent cutting regime ($f = 0.4$ mm/rev and $V_C = 800$ m/min) [33].

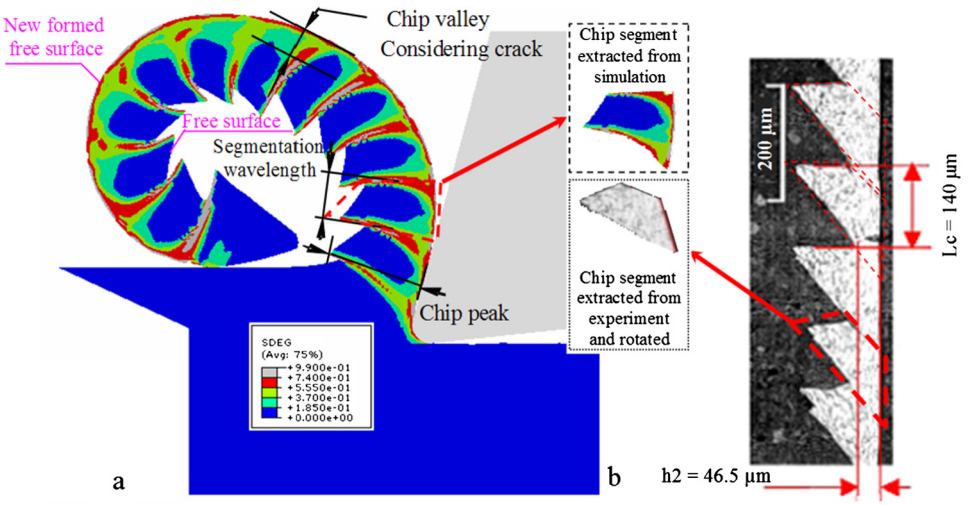

Fig. 15. Chip morphology ($V_C = 120$ m/min, $f = 0.127$ mm/rev, $\mu = 0.7$), a) numerical simulation [48], b) experimentation [50].

Table 2
Chip morphology and forces obtained experimentally and numerically. Here the cutting edge radius is $r_\beta = 30$ µm, approximately.

$V_C = 120$ m/min	L_C (µm)	Pick (µm)	Valley (µm)	F_C (N) [49]
Experience [50]	140	165	46.5	559.0
Simulation	133 ± 8	162 ± 7	48.0 ± 19.0	541.3
Error (%)	−5	−2	4.4	−3.2

stresses fall and the equivalent plastic strain increases. Moreover, localized damage takes place on chip free surface. In the final stage, the damage is extended along the primary shear zone due to the excessive compression state. So, according to this result, the segmentation is the result of a softening state during tool–workpiece interaction. Nevertheless, this is not the only phenomenon yielding to the chip segmentation; other phenomena can participate in the formation of the sawtooth chip shape, such as pre-existing micro-cracks, machine tool vibrations [47] or/and the nature of the chip–workpiece contact.

Moreover, it is important to underline that the comprehension of residual stress distributions after machining operations is of great interest to industry because their values and orientations can affect the functional mode of the whole machined part in a global given mechanical system. This numerical model seems to be a useful solution for predicting residual stress in machining [33].

The same approach was adopted during the elaboration of the cutting model of titanium alloy Ti-6Al-4V. Here, a user routine *VFRIC* was elaborated in order to define the interfacial limiting shear stress as a function of temperature, strain, and strain rate [48]. After that, the friction model of Zorev [45] was integrated into the modelling for the simulation of the cutting of titanium alloy Ti-6Al-4V. The numerical result obtained (Fig. 15) for $V_C = 120$ m/min, $f = 0.127$ mm/rev and $\mu = 0.7$ was compared to an experimental one given in [49]. It appears that, in these conditions, the formation of a chip segment occurs following the initiation of a crack that starts at the chip free surface and moves towards the side of the tool-tip. Generally, corroboration between experimental and numerical can be mentioned. Table 2 summarises the obtained geometric results carried out on both experimental and numerical chips.

4.2. Cutting model for down-cut peripheral milling

The previously elaborated model was exploited to build a cutting model in the case of down-cut peripheral milling of the A2024 aluminium alloy. Here, the objective is to highlight the influence of the machining system's vibrations on

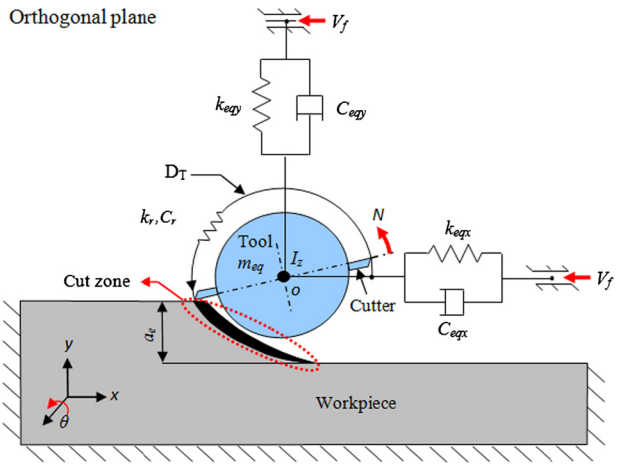

Fig. 16. Schematic representation of down-cut peripheral milling (HDC-model).

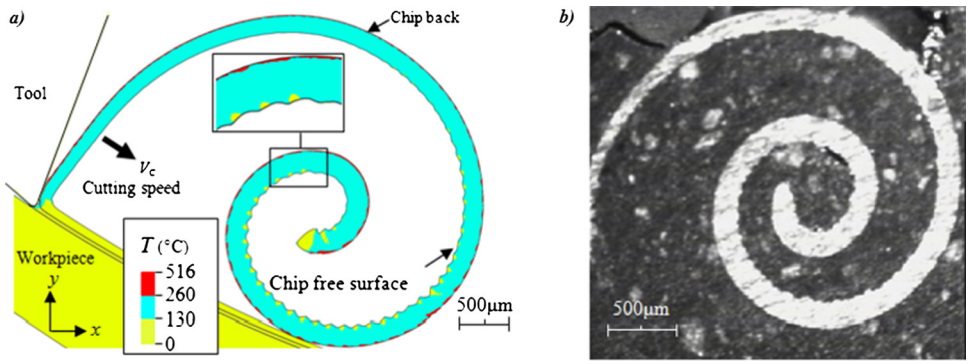

Fig. 17. Chip morphology ($V_C = 800$ m/min, $f = 0.2$ mm/rev); a) numerical simulation b) experimentation [51].

chip formation and in particular on the tool–workpiece interaction. For this, a cutting model named Hybrid Cutting Model (HDC-model) [51] was elaborated with the ABAQUS®/Explicit software. For that, the machining system (here the milling spindle: tool, tool holder and rotor) is modelled by an equivalent mass m_{eq}, an equivalent stiffness k_{eq}, and an equivalent damping C_{eq}. The workpiece is modelled by a continuum material. A schematic representation of the HDC-model is given in Fig. 16. Based on HDC, a parametric study highlighting the effect of the stiffness and damping of the machining system on the chip formation was performed.

Cutting simulations without vibrations were carried out at $V_C = 800$ m/min and $f = 0.2$ mm/rev. The morphology of the obtained chip is very similar to that obtained experimentally (Fig. 17). The maximum temperature for this calculation is located in a layer situated in the chip back. Initially, the simulated chip has small segments that disappear towards the end with decreasing thickness. It is remarked that the softening effect is not very important for these cutting conditions and for the material concerned.

In the same cutting conditions and for a tool angular position of 22° and when passing from stiffness values of $2 \cdot 10^7$ N/m to $20 \cdot 10^7$ N/m, the HDC model shows a decrease in chip segmentation (Fig. 18). Also, it should be noted that the wavelength of the segments remains almost the same for the two stiffness values. For more details on the HDC model, the reader is referred to paper [51].

In summary, based on the obtained results, it can be underlined that a machining system with high stiffness and/or high structural damping promotes a decrease in chip segmentation. Nevertheless, increasing the cutting speed induces strongly the segmentation phenomenon yielding to the vibration of the machining system All this shows how, for the cutting conditions in HSM, to set a suitable choice of cutting parameters and characterising the machining system (spindle, bearings, tool, tool-holder, etc.).

4.3. Cutting model based on the theory of gradient plasticity

It is now well established by experimental analysis that the response of the material, under complex loadings, varies with the size of the specimens. As the sample size is small, the more the material resists. Similarly, for cutting, it is well established, and for a long time ago, that the closer the minimum chip thickness, the more specific the value of cutting energy is high. Hence, the research for an appropriate constitutive law to describe efficiently the passage at scales limits has

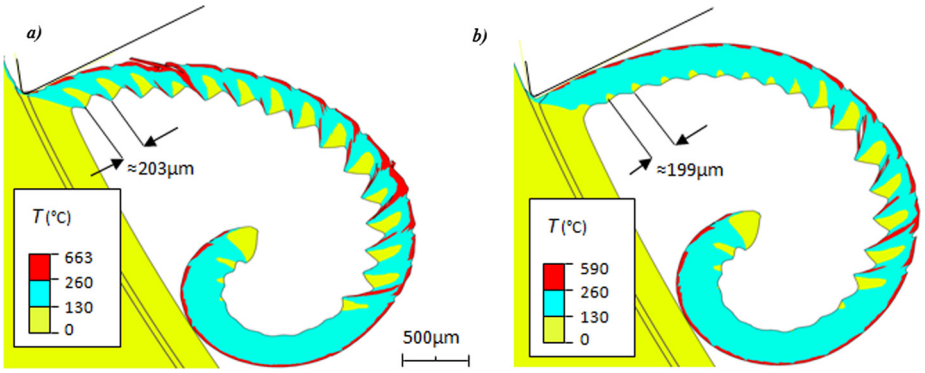

Fig. 18. Simulated chip morphology (HDC-model) ($V_C = 800$ m/min, $f = 0.2$ mm/rev); a) $k_{eq} = 2 \cdot 10^7$ N/m, b) $k_{eq} = 20 \cdot 10^7$ N/m.

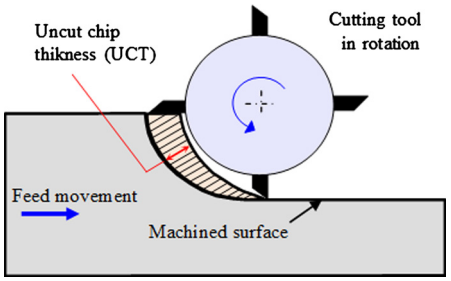

Fig. 19. Schematic representation of the down-cutting peripheral milling.

to be accomplished. This law must integrate the so-called "scale effect". The use of second gradient theory can be adopted in order to modify the Johnson–Cook constitutive model as it was proposed in [51]. To illustrate the usefulness of this in a practical perspective, it can be noted for example that, in down-cut peripheral milling, the machined surface is mainly created when the removal of material occurs in the thinnest zone of the chip, with micrometric thickness and scale (Fig. 19).

This gradient theory has been developed for the first time in the early 1960s through the work of [52,53] for a continuous medium. More details on the elaborated model in the case down-cut peripheral milling was developed in [54]. The new constitutive law proposed has been implemented in ABAQUS®/Explicit via a user routine *VUMAT* it concerns the modified Johnson–Cook, which is given by the equation:

$$\bar{\sigma} = \bar{\sigma}_{JC}\sqrt{1 + \left(\frac{18\alpha^2 G^2 b\eta}{\bar{\sigma}_{JC}^2}\right)^{\chi}} = \bar{\sigma}_{JC}\sqrt{1 + (l\eta)^{\chi}} \tag{10}$$

where b is the Burgers vector, G is the material shear modulus, χ is the geometric factor defining the density (GND) of the geometrically necessary dislocations, α_t is Taylor's constant, η is a strain gradient coefficient, and l is an intrinsic characteristic length of the cut material, which is defined in the literature as $l = 18(\frac{\alpha G}{\bar{\sigma}_{JC}})^2 b$.

The obtained numerical results were compared with experimental ones (Fig. 20) in terms of the variations of the calculated and measured specific cutting energies (defined as cutting force divided by chip thickness) as a function of the uncut chip thickness (UCT) and for the four considered cutting speeds V_C. The plots concerning the results showed in Fig. 20 show a narrow evolution of the specific cutting energy when the cutting speed increases. Practically, this result is well known for the concerned aluminium alloy. The variations are sensitive only below 300 m/min, for the values tested here. This remark confirms that this experiment can be considered as a good reference for numerical comparisons.

According to Fig. 20, the differences with experiments vary from 100 to 500 MPa for the simulation without SG. These variations are reduced between 0 and 100 MPa when the SGP approach is adopted. This clearly shows that the consideration of the SGP effect improves the quality of the numerical results.

It is noticeable that the desired correction for small thicknesses (20 µm in our application) has also an effect for higher uncut chip thicknesses (200 µm and more). This highlights the number and the complexity of the basic physical phenomena to be considered to simulate the violence of the occurring physical phenomena met in metal cutting

In summary, experimental results validate adequately the numerical ones and confirm clearly the relevance of the adoption of strain gradient plasticity in capturing scale effect.

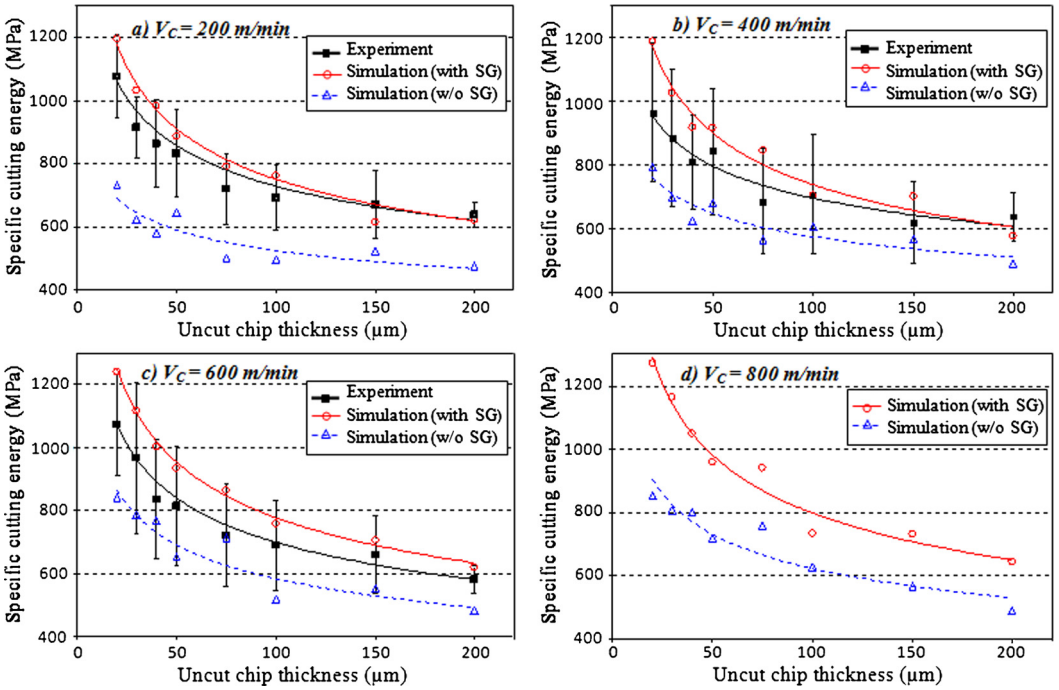

Fig. 20. Specific cutting energy versus uncut ship thickness, for different cutting speed values (material A2024).

5. Conclusion

All the results presented above confirm the valuable integration of modelling and simulations in the chain of the workpiece's life cycle. Indeed, the major scientific obstacle to the cutting process' optimization and monitoring is mainly in relationship with the physical understanding level of the tool–workpiece interaction. Simulation helps fulfil a technological leap in providing added values to all processes and in particular in the field of material removal. The obtained simulation results are of course relevant as the models are powered by faithfully input established laws and also based on the robustness of numerical methods.

In machining and particularly in turning, it is better to have fragmented chips. Most manufacturers propose an operating domain characterizing the chip fragmentation for a given workpiece–tool pair, commonly called "chip breaker diagram". Through the presented models, it can be underlined that chip segmentation can be an initiator for this fragmentation. Nevertheless, it can be remarked that chip segmentation generates the oscillation of the cutting forces and causes geometrical defects on the machined surface and a non-uniform distribution of residual stresses. Based on what has been published up to now in the field of numerical cutting, it can be said that simulation is an essential mean to understand the tool–workpiece interaction even in a traditional way by elaborating a Numerical Couple Workpiece Tool (CWT) methodology [3] by analogy to the experimental CWT.

Moreover, it can be noted that phenomenological constitutive material laws are interesting to feed cutting models, but they have a lack because they do not they do not describe finely the tool–workpiece interaction, especially when micro-sizes are reached. Studies based on crystal plasticity or the strain gradient plasticity may give a better vision and lead to a more precise physical understanding of phenomena. For example, through this paper, it appears that in the case of down-cut peripheral milling where the chip reaches micrometre thickness, the size effect has to be considered in the constitutive law to faithfully capture material hardening. This can help adequately simulate the machining process and thus, for example, capture the evolution of the specific cutting energy with the variation of chip thickness.

Eventually, it can be said that continuing to model more finely the material thermomechanical behaviour and presenting the tool–workpiece interaction adequately can certainly contribute to an advanced theoretical understanding of material removal using a cutting tool.

References

[1] Y. Kaynak, S.W. Robertson, H.E. Karaca, I.S. Jawahir, Progressive tool-wear in machining of room-temperature austenitic NiTi alloys: the influence of cooling/lubricating, melting, and heat treatment conditions, J. Mater. Process. Technol. 215 (2015) 95–104.

[2] M. Nouari, M. Calamaz, F. Girot, Wear mechanisms of cutting tools used in the dry machining of the aeronautic titanium alloy, Ti-6Al-4V, C. R., Méc. 336 (10) (2008) 772–781.

[3] AFNOR, NF E 66-520-1, "Working zones of cutting tools – Couple tool-material – Part 1: general presentation", French Standard, ISSN 0335-3931, Sept. 1997.

[4] G.G. Ye, S.F. Xue, M.Q. Jiang, X.H. Tong, L.H. Dai, Modeling periodic adiabatic shear band evolution during high speed machining Ti-6Al-4V alloy, Int. J. Plast. 40 (2013) 39–55.
[5] X.P. Zhang, R. Shivpuri, A.K. Srivastava, Role of phase transformation in chip segmentation during high speed machining of dual phase titanium alloys, J. Mater. Process. Technol. 214 (12) (2014) 3048–3066.
[6] T. Childs, K. Maekawa, T. Obikawa, Y. Yamane, Metal Machining: Theory and Applications, John Wiley & Sons Inc., ISBN 0-340-69159-X, 2000, 408 pp.
[7] H. Tresca, On further applications of the flow solids, in: Proceedings of the Institute of Mechanical Engineers, vol. 30, 1878, pp. 301–345.
[8] P.Y. Sevilla-Camacho, J.B. Robles-Ocampo, J.C. Jauregui-Correa, D. Jimenez-Villalobos, FPGA-based reconfigurable system for tool condition monitoring in high-speed machining process, Measurement 64 (March 2015) 81–88.
[9] J. Barry, G. Byrne, The mechanisms of chip formation in machining hardened steels, J. Manuf. Sci. Eng. 124 (2002) 528–535.
[10] S. Belhadi, T. Mabrouki, J.-F. Rigal, L. Boulanouar, Experimental and numerical study of chip formation during straight turning of hardened AISI 4340 steel, Proc. Inst. Mech. Eng., B J. Eng. Manuf. 219 (2005) 515–524.
[11] G. Poulachon, A. Moisan, A contribution to the study of the cutting mechanisms during high speed machining of hardened steel, CIRP Ann. 47 (1) (1998) 73–76.
[12] C. Courbon, Vers une modélisation physique de la coupe des aciers spéciaux: intégration du comportement métallurgique et des phénomènes tribologiques et thermiques aux interfaces, PhD thesis, Ecole Centrale de Lyon, 2011.
[13] Z.-B. Hou, R. Komanduri, On a thermomechanical model of shear instability in machining, CIRP Ann. 44 (1) (1995) 69–73.
[14] C. Courbon, T. Mabrouki, J. Rech, D. Mazuyer, F. Perrard, E. D'Eramo, Further insight into the chip formation of ferritic-pearlitic steels: microstructural evolutions and associated thermo-mechanical loadings, Int. J. Mach. Tools Manuf. 77 (2014) 34–46.
[15] J.A.B. VanDijck, The direct observation in the transmission electron microscope of the heavily deformed surface layer of a copper pin after dry sliding against a steel ring, Wear 42 (1977) 109–117.
[16] M. Vaz Jr., D.R.J. Owen, V. Kalhori, M. Lundblad, L.M. Lindgren, Modelling and simulation of machining processes, Arch. Comput. Methods Eng. 14 (2) (2007) 173–204.
[17] M. Barge, H. Hamdi, J. Rech, J.M. Bergheau, Numerical modelling of orthogonal cutting: influence of numerical parameters, J. Mater. Process. Technol. 164 (2005) 1148–1153.
[18] Y. Ohbuchi, T. Obikawa, Adiabatic shear in chip formation with negative rake angle, Int. J. Mech. Sci. 47 (9) (2005) 1377–1392.
[19] T. Özel, T. Altan, Process simulation using finite element method-prediction of cutting forces, tool stresses and temperatures in high-speed flat end milling, Int. J. Mach. Tools Manuf. 40 (5) (2000) 713–738.
[20] M. Movahhedy, S. Gadala, Y. Altintas, Simulation of the orthogonal metal cutting process using an arbitrary Lagrangian–Eulerian finite-element method, J. Mater. Process. Technol. 103 (2) (2000) 267–275.
[21] M.N.A. Nasr, E.G. Ng, M.A. Elbestawi, Modelling the effects of tool-edge radius on residual stresses when orthogonal cutting AISI 316L, Int. J. Mach. Tools Manuf. 47 (2007) 401–411.
[22] C. Bonnet, F. Valiorgue, J. Rech, C. Claudin, H. Hamdi, J.M. Bergheau, P. Gilles, Identification of a friction model – application to the context of dry cutting of an AISI 316L austenitic stainless steel with a TiN coated carbide tool, Int. J. Mach. Tools Manuf. 48 (11) (2008) 1211–1223.
[23] E. Ceretti, M. Lucchi, T. Altan, FEM simulation of orthogonal cutting: serrated chip formation, J. Mater. Process. Technol. 95 (13) (1999) 17–26.
[24] D. Umbrello, J. Hua, R. Shivpuri, Hardness-based flow stress and fracture models for numerical simulation of hard machining AISI 52100 bearing steel, Mater. Sci. Eng. A 374 (1–2) (2004) 90–100.
[25] G.C. Johnson, D.J. Bammann, A discussion of stress rates in finite deformation problems, Int. J. Solids Struct. 20 (8) (1984) 725–737.
[26] S. Jing, C.R. Liu, The influence of material models on finite element simulation of machining, J. Manuf. Sci. Eng. 126 (4) (2004) 849–857.
[27] Y.B. Guo, A FEM study on mechanisms of discontinuous chip formation in hard turning, J. Mater. Process. Technol. 155 (2004) 1350–1356.
[28] M. Calamaz, J. Limido, M. Nouari, C. Espinosa, D. Coupard, M. Salaün, F. Girot, R. Chieragatti, Toward a better understanding of tool wear effect through a comparison between experiments and SPH numerical modelling of machining hard materials, Int. J. Refract. Met. Hard Mater. 27 (2009) 595–604.
[29] M. Sima, T. Özel, Modified material constitutive models for serrated chip formation simulations and experimental validation in machining of titanium alloy Ti-6Al-4V, Int. J. Mach. Tools Manuf. 50 (11) (2010) 943–960.
[30] M. Hashimura, Y.P. Chang, D. Dornfeld, Analysis of burr formation in orthogonal cutting, J. Manuf. Sci. Eng. 121 (1) (1999) 1–7.
[31] Y.B. Guo, D.A. Dornfeld, Finite element modeling of burr formation process in drilling 304 stainless steel, J. Manuf. Sci. Eng. 122 (4) (2000) 612–619.
[32] A. Ramesh, Prediction of process-induced microstructural changes and residual stresses in orthogonal hard machining, PhD dissertation, Georgia Institute of Technology, 2002.
[33] T. Mabrouki, F. Girardin, M. Asad, J.F. Rigal, Numerical and experimental study of dry cutting for an aeronautic aluminium alloy (A2024-T351), Int. J. Mach. Tools Manuf. 48 (11) (2008) 1187–1197.
[34] S. Subbiah, S.N. Melkote, Effect of finite edge radius on ductile fracture ahead of the cutting tool edge in micro-cutting of Al2024-T3, Mater. Sci. Eng. A 474 (1–2) (2008) 283–300.
[35] O. Abiri, L.E. Lindgren, Non-local damage models in manufacturing simulations, Eur. J. Mech. A, Solids 49 (2015) 548–560.
[36] A. Hillerborg, M. Modéer, P.E. Petersson, Analysis of crack formation and crack growth in concrete by means of fracture mechanics and finite elements, Cem. Concr. Res. 6 (1976) 773–782.
[37] J.R. Rice, D.M. Tracey, On the ductile enlargement of voids in triaxial stress fields, J. Mech. Phys. Solids 17 (2) (1969) 201–217.
[38] J. Lemaitre, R. Desmorat, Engineering Damage Mechanics, Ductile, Creep, Fatigue and Brittle Failures, Springer, Berlin, Heidelberg, 2005, pp. 10–12.
[39] ABAQUS®/EXPLICIT, Theory and user manuals, Version 6.7.1, 2007.
[40] M. Bäker, J. Rösler, C. Siemers, A finite element model of high speed metal cutting with adiabatic shearing, Comput. Struct. 80 (5–6) (2002) 495–513.
[41] T. Mabrouki, J.F. Rigal, A contribution to a qualitative understanding of thermo-mechanical effects during chip formation in hard turning, J. Mater. Process. Technol. 176 (2006) 214–221.
[42] Q. Wen, Y.B. Guo, B.A. Todd, An adaptive FEA method to predict surface quality in hard machining, J. Mater. Process. Technol. 173 (1) (2006) 21–28.
[43] R.F. Recht, Catastrophic thermoplastic shear, J. Appl. Mech. 86 (1964) 189–193.
[44] H.J. Frost, M.F. Ashby, Deformation-Mechanism Maps, Pergamon Press, Elmsford, 1982, pp. 1–16.
[45] N. Zorev, Inter-relationship between shear processes occurring along tool face and shear plane in metal cutting, in: Transaction of the ASME, International Research in Production Engineering, 1963, pp. 42–49.
[46] H. Jiang, R. Shivpuri, Prediction of chip morphology and segmentation during the machining of titanium alloys, J. Mater. Process. Technol. 150 (1–2) (2004) 124–133.
[47] M. Asad, T. Mabrouki, F. Girardin, Y. Zhang, J.F. Rigal, Towards a physical comprehension of material strengthening factors during macro to micro-scale milling, Mechanika (ISSN 1392-1207) 17 (1) (2011) 97–104.
[48] Y. Zhang, T. Mabrouki, D. Nelias, Y. Gong, Chip formation in orthogonal cutting considering interface limiting shear stress and damage evolution based on fracture energy approach, Finite Elem. Anal. Des. 47 (2011) 850–863.
[49] D. Umbrello, Finite element simulation of conventional and high speed machining of Ti-6Al-4V alloy, J. Mater. Process. Technol. 196 (1–3) (2008) 79–87.
[50] H. Jiang, R. Shivpuri, Prediction of chip morphology and segmentation during the machining of titanium alloys, J. Mater. Process. Technol. 150 (1–2) (2004) 124–133.

[51] M. Asad, T. Mabrouki, J.-F. Rigal, Finite-element-based hybrid dynamic cutting model for aluminium alloy milling, Proc. Inst. Mech. Eng., B J. Eng. Manuf. 224 (B1) (2010) 1–13.
[52] R.A. Toupin, Elastic materials with couple stresses, Arch. Ration. Mech. Anal. 11 (1962) 358–414.
[53] R.D. Mindlin, Second gradient of strain and surface tension in linear elasticity, Int. J. Solids Struct. 1 (1965) 417–438.
[54] M. Asad, Elaboration of concepts and methodologies to study peripheral down-cut milling process from macro-to-micro scales, PhD thesis, INSA of Lyon, France, 2010.